Surface Core-Level Shifts as a Toolbox to Evidence the BaTiO 3 Ferroelectric Phase Transition

Amit Sahu, Pierre-Marie Deleuze, Hélène Magnan, Antoine Barbier, Zheshen Li, Sylvie Bourgeois, Bruno Domenichini, Céline Dupont

Surface Core-Level Shifts as a Toolbox to Evidence the $BaTiO_3$ Ferroelectric Phase Transition

Amit Sahu,[†] Pierre-Marie Deleuze,[†] Hélène Magnan,[‡] Antoine Barbier,[‡] Zheshen Li,[¶] Sylvie Bourgeois,[†] Bruno Domenichini,[†] and Céline Dupont[*,†]

[†]*Laboratoire Interdisciplinaire Carnot de Bourgogne, UMR 6303 CNRS-UBFC, 21078 Dijon Cedex, France*

[‡]*Université Paris-Saclay, CEA, CNRS, Service de Physique de l'Etat Condensé, 91191 Gif-sur-Yvette, France*

[¶]*ISA, University of Aarhus, DK-8000 Aarhus C, Denmark*

E-mail: celine.dupont@u-bourgogne.fr

Abstract

We predict by Density Functional Theory (DFT) calculations structural modifications specific of the paraelectric/ferroelectric transition and demonstrate that they can be tracked experimentally by means of Photoelectron Spectroscopy (PES). For $BaTiO_3$, we evidence that the Ba 4*d* core-level binding energy shifts conveniently allow to track the transition for both approaches. DFT calculations reveal different temperature behaviors for bulk and surface features, which can be experimentally followed by PES thanks to specific core-level shifts. Consistently, our PES data show that such modifications occur at a temperature close to the ferroelectric (*P4mm*)→ paraelectric (*Pm3m*) phase transition of $BaTiO_3$. We thus demonstrate that a fine PES investigation of the electronic structure can be used to evidence a ferroelectric to paraelectric

phase transition. These results are believed to be general for ferroelectric surfaces and it is shown that this approach is applicable to other ferroelectric titanate compounds.

Introduction

In recent years, ferroelectric materials have gained a lot of attention due to their promising use in many technological applications such as non-volatile memory devices,[1] capacitors[2] or photocatalysts.[3,4] Barium titanate ($BaTiO_3$) is a prototypical ferroelectric, it was the first ceramic material discovered exhibiting ferroelectricity.[5] At room temperature, $BaTiO_3$ has a tetragonal *P4mm* structure where the Ba^{2+} ions are at the corners, the O^{2-} ions at the center of the faces and the Ti^{4+} ion at the body center. The non-centrosymmetric unit cell allows the material to be ferroelectric thanks to the displacements of Ti and O atoms inducing a net dipole moment and therefore an electric polarization. Around 130°C, bulk $BaTiO_3$ undergoes a phase transition towards a cubic *Pm3m* paraelectric phase.[6–8] The phase transitions in $BaTiO_3$ have been thoroughly investigated over decades by different techniques[9–13] such as Raman spectroscopy,[14] X-ray diffraction (XRD)[15,16] or extended X-ray absorption spectroscopy (EXAFS).[17] However, to the best of our knowledge, the surface region behavior during the transition has not yet been investigated in much details by X-ray Photoelectron Spectroscopy (PES). This might come from two reasons: (i) on the one hand, this material is an insulator and thus subject to charge build-up effects detrimental to photoemission investigations; (ii) on the other hand, $BaTiO_3$ is often found in powder or sintered polycrystalline forms which prevents an accurate control of the polarization direction, this latter being random for each particle. Here we show that synchrotron radiation X-ray Photoelectron Spectroscopy (SR-PES) provides a specific signature allowing to tackle this issue.

In this work we use Density Functional Theory (DFT) to study the evolution of core level binding energy shifts of Ba 4*d* components of different slabs of $BaTiO_3$. Very thin (*i.e.* avoiding charging effects) epitaxial films of single crystalline $BaTiO_3$ are then analyzed ex-

perimentally upon increasing temperature by means of surface sensitive SR-PES, in order to complement our calculations.

Methods

DFT calculations have been performed using the Vienna *ab initio* simulation package (VASP)[18,19] under periodic boundary conditions. The electron-ion interaction is described within the projector-augmented plane-wave (PAW) method[20] with a kinetic energy cutoff of 500 eV and the inclusion of ten valence electrons for Ba, six for O, and four for Ti. The generalized gradient approximation (GGA) is employed with the Perdew-Burke-Ernzerhof (PBE)[21] exchange-correlation functional. The DFT+U approach is used by including an on-site Coulomb repulsion U-term for the Ti 3d electrons, according to the Dudarev method.[22] The effective parameter U_{eff} = 3.5 eV is applied, increasing the band gap from 1.85 to 2.23 eV, getting closer to the experimental value of 3.2 eV.[23] The convergence threshold on total energy is set to 10^{-6} eV. The structural optimization is stopped when the forces converged below 0.01 eV.Å^{-1}, while a 7×7×1 Monkhorst-Pack[24] k-point mesh is used to sample the first Brillouin zone. By consistency with our previous results, $BaTiO_3$(001) is modeled only with a BaO termination.[25] Starting from the bulk parameter previously obtained,[26] namely $a = 4.006$ Å, slabs of different a' values ranging from 3.80 to 4.10 Å are used in order to model the influence of compressive and tensile strains. Besides (2×1) unit cells are used to model the polarization while avoiding depolarizing field (see[26] and references therein for further details). Eleven layers symmetric slabs, with all atoms allowed to relax, are systematically considered in either paraelectric or ferroelectric or both configurations, with a vacuum space of 20 Å along the z axis.

For the experimental approach, $BaTiO_3$ films were epitaxially grown by Oxygen Plasma Assisted Molecular Beam Epitaxy (OA-MBE),[25,27] on 1% Nb doped $SrTiO_3$ single crys-

tals. Such substrates are conductive enough to avoid charge build-up during spectroscopy measurements. The Nb:$SrTiO_3$ substrates are 5 × 5 mm squares with a thickness of 1 mm, provided by Crystal GmBH (Berlin, Germany). The OA-MBE method allows the deposition of single crystalline layers of controlled morphology, stoichiometry and thickness. Dedicated Knudsen cells are used to evaporate high-purity Ba and Ti (99.99% grade) metals in the presence of an atomic oxygen plasma (high brilliance, 350 W power). Well-defined oxides are obtained under good vacuum conditions (10^{-7} mbar working pressure, 10^{-10} mbar base pressure). In order to clean the substrate, Nb:$SrTiO_3$(001) is first heated under oxygen plasma (RF power 350 W) during one hour prior to the deposition at 450°C, with a filament located behind the sample. The sample was held at 450°C during the growth. Two samples of different thicknesses (10 and 16 nm) were prepared with the BaO termination. The thickness is chosen such as to allow a full structural relaxation[28] of the layers in order to avoid substrate clamping effects known to alter the Curie temperature. Surface termination is tuned by closing the shutter of the Ti evaporator 4 minutes prior to the Ba one, considering atomic flux of 2 Å/min.

The growth and the quality of the films were then controlled during growth *in situ* by Reflection High-Energy Electron Diffraction (RHEED). SR-PES experiments were carried out at the Aarhus storage ring in Denmark (ASTRID2) on the Matline beamline, dedicated to surface analysis and equipped with a SX700 grating monochromator. The end-station consists of a mu-metal UHV chamber, a hemispherical SPECS Phoebios-150 electron energy analyzer. The set-up offers an overall resolution of *ca.* 60 meV at 75 eV kinetic energy. The temperature was measured by a thermocouple fixed on the sample surface. Prior to SR-PES experiments, we cleaned the samples by an annealing at 400°C under 10^{-6} mbar of oxygen for one hour. In order to check the cleanliness of the surface at different stages of the preparation, we recorded large energy scans using a photon energy of 400 eV in order to be very sensitive to the surface. Within a simple layer model, the relative peak intensities of C 1s, Ba 4d and Ti 3p allow to estimate the C thickness. We found a carbon thickness

below *ca.* 1/5 monolayer, which stands for a reasonably clean surface (see Supplementary Information). For the Ba 4*d* and Ti 3*p* core-level recordings discussed here the photon energy was set to 160 eV. Spectra were recorded at normal take-off angle, while the data were analyzed using the CasaXPS software.[29] A Shirley background was employed for the fitting process and 70% Gaussian/30% Lorentzian peak shapes. This method of XPS line fitting has been tested previously and is described in detail in a previous paper where we identified unambiguously the nature of the Ba 4*d* peak contributions in $BaTiO_3$.[25]

Results

DFT calculations were performed on samples experiencing different compressive and tensile strains, for the ferroelectric and paraelectric states. Specifically, BaO terminated slabs with in-plane lattice parameters a' ranging from 3.80 Å (compressive stress) to 4.10 Å (tensile stress) have been considered. This evolution of the lattice parameter has been chosen to mimic an experimental increase of temperature within reasonable strain boundary conditions. Thus, we have considered ferroelectric slabs with lattice parameters of 3.80 Å, 3.85 Å, and 3.90 Å only, since lower strains (*i.e.* a' closer to the bulk value) do not allow to obtain a clear ferroelectric state. Higher stresses with a' lower than 3.80 Å have not been considered because a a' value of 3.75 Å would already correspond to a strain higher than 6% (a value difficult to reach experimentally). Moreover, theoretically a paraelectric slab cannot be obtained under such a strain. For the paraelectric part of the phase diagram, the same values of a' (namely 3.80 Å, 3.85 Å and 3.90 Å) were investigated and additionally a non-strained slab (*i.e.* with the native lattice parameter of 4.006 Å) and one case of tensile strain (a'=4.10 Å) to mimic high experimental temperatures.

For all models, core-level binding energies were calculated in the final state approximation, to simulate electronic structure and PES evolution, following the method developed by Köhler and Kresse.[30] However, since the screening of the core electrons is not taken into

account, this approach can only provide core-level binding energies shifts. As demonstrated previously,[25] Ba $4d$ presents two components: one called α related to bulk Ba atoms and another one called β, corresponding to Ba atoms from the top surface layer. We report the theoretical evolution of the binding energy difference between these two components in Figure 1 for all ferro/paraelectric states and lattice parameters listed above.

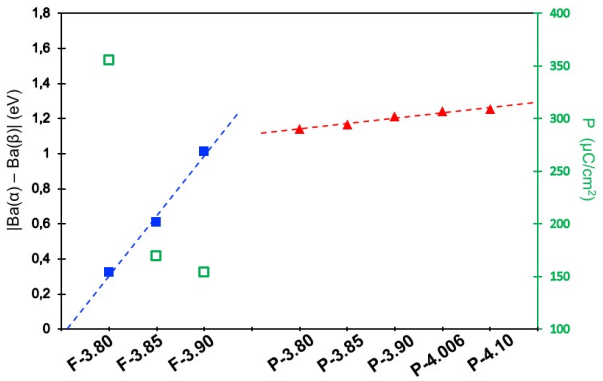

Figure 1: (Left axis) Theoretical evolution of the $|Ba(\alpha) - Ba(\beta)|$ energy difference (in eV) as a function of ferroelectricity and lattice parameter. For values in abscissa, F stands for a ferroelectric slab, while P corresponds to the paraelectric one. Numbers next to P or F indicate the lattice parameter in Å. Values for ferroelectric slabs are reported with blue squares, while red triangles stand for paraelectric slabs. Blue and red dotted lines are eye guidelines and correspond to linear regressions for ferro and paraelectric data, respectively. (Right axis) Total polarization of each ferroelectric slab in μC/cm^2 (green open squares).

According to Figure 1, the ferro and paraelectric slabs clearly exhibit different behaviors with respect to the shift between the Ba(α) and Ba(β) components. For ferroelectric slabs, the shift increases with a rather important slope ($\approx$ 6.9 eV/Å) when the strain is reduced while for the paraelectric slabs, the slope is approximatively 10 times smaller ($\approx$ 0.6 eV/Å). For the ferroelectric cases, the total polarization has been calculated following the formula developed by Vanderbilt,[31] which has been already applied in reference.[26] In this model, the local polarization is calculated for each unit cell centered on a Ti atom for the configuration exhibiting the BaO termination. The total polarization, reported in Figure 1 (Right axis), is then obtained by summing the local polarizations over the whole slab. These results show that the theoretical PES shift between the two Ba components is clearly dependent on the ferro/paraelectric state. Moreover, the ferroelectric state appears as fairly more sensitive to

strain and polarization. In order to validate these calculations, we measured experimentally the evolution of the Ba 4*d* PES peak of epitaxial thin layers of $BaTiO_3$ as a function of the temperature across the ferro/paraelectric transition. First, the structure of the samples was investigated by RHEED. Both samples exhibit very similar RHEED patterns, like the ones reported in Figure 2 for the 10 nm thick samples. It features straight streaks in the $[10]^*$ and $[11]^*$ reciprocal space directions indicating an epitaxial two-dimensional growth of the $BaTiO_3$ overlayer.

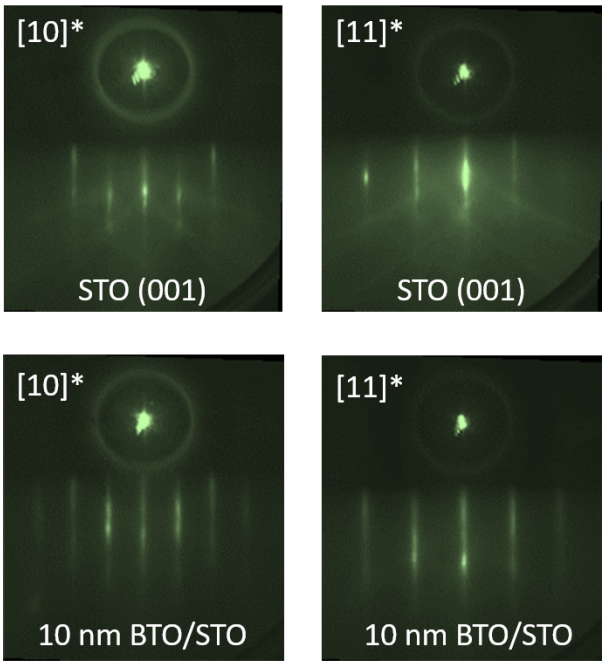

Figure 2: (Left panel) RHEED patterns over the $[10]^*$ reciprocal space direction (in surface lattice units) of the $SrTiO_3$ substrate (Top) and after 10 nm thick $BaTiO_3$ deposition (Bottom). (Right panel) RHEED patterns over the $[11]^*$ reciprocal space direction of the STO substrate (Top) and after 10 nm thick $BaTiO_3$ deposition (Bottom).

After checking the cleanliness of the surface, the evolution of the PES spectra is followed as a function of temperature. To do so, the Ba 4*d* and Ti 3*p* core-levels were recorded at temperatures ranging from room temperature up to 300°C. Spectra obtained at 50°C and 300°C are reported in Figure 3. We used a XPS fitting method that has been described in detail in our previous paper[25] where we demonstrated that the Ba 4*d* lines can be decomposed into Ba 4*d* 5/2 and Ba 4*d* 3/2 lines separated by a spin orbit coupling of 2.6 eV each

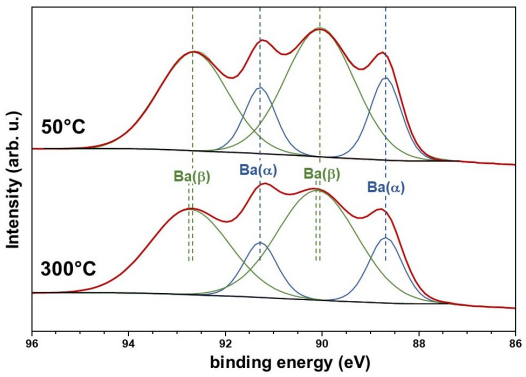

Figure 3: Ba 4*d* spectra recorded at two temperatures: (Top) 50°C (Bottom) 300°C. Ba 4*d* lines are decomposed into two components: Ba(β) in green and Ba(α) in blue.

having two components (α and β). Additional constraints include larger Full Widths at Half Maximum (FWHMs) for β components than for α ones, which are found to depend slightly on temperature (see Supplementary Information) in order to ensure a unique decomposition. The validity of this method has been tested for different incidence angles (see Supplementary Information) and allows to demonstrate that only four peaks are necessary to fit XPS spectra for all conditions (e.g. different surface terminations, incidence angles or temperatures). Before discussing the effect of temperature, let us discuss the difference in FWHM for Ba(β) and Ba(α). An increase of the FWHM can be due to charging effect, hole lifetime increase or different chemical environment. In our case, charging or hole lifetime effects can be discarded since they are identical for both peaks. From reference,[25] we know that Ba(β) peaks are due to BaO surface species, which has a sizeable impact on the peak width as we will detail hereafter. Crystal Orbital Hamilton Population (COHP)[32] and chemical bonding analysis[33] have been performed thanks to the LOBSTER code.[34] The corresponding results are reported in Figure 4. COHP analysis allows to discriminate anti-bonding (left side of each plot) and bonding (right side) states: a higher amount of bonding states indicates a greater stability. The crossing point between bonding and anti-bonding states thus evolves as stability. According to Figure 4, the crossing points (dotted lines) are at higher energy for surface Ba-O bonds than for bulk ones, for both paraelectric and ferroelectric slabs. This

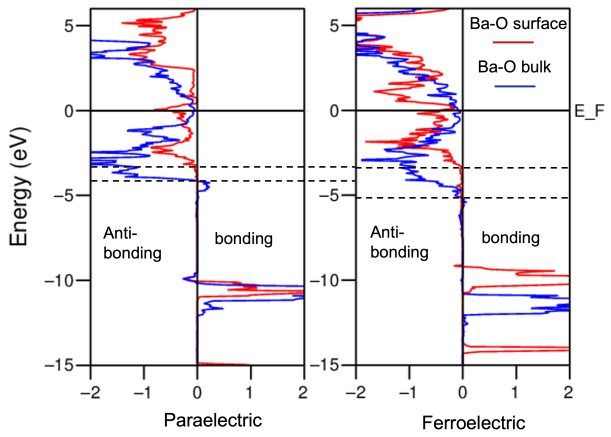

Figure 4: COHP analysis for (Left) paraelectric and (Right) ferroelectric slabs. Blue lines correspond to Ba-O bulk bonds, while red ones are related to surface Ba-O ones. Dotted lines allow to identify the crossing point between bonding and anti-bonding states. The zero of the energy scale is set to be the respective Fermi energy.

result indicates that the BaO top layer is always bonded more weakly than the BaO layers in the bulk. This can thus induce a greater flexibility of the top layer, allowing a wider dispersion leading to the broadening of Ba(β) peaks. It is worthy to note that the crossing point for surface Ba-O hardly changes between ferro and paraelectric slabs, indicating similar chemical environments of the surface Ba atoms whatever the ferro/paraelectric state is.

In order to reduce the uncertainties induced by the change in photon energy and/or charging effects, we choose to follow the evolution of the PES spectra by comparing relative binding energy positions. Thus, we represent the Ba 4d PES lines as a function of the difference in kinetic energy with respect to the position of the Ti 3p line recorded on the same sample at the same temperature. By comparing different temperatures, one can see modifications in the Ba 4d PES spectra when the temperature increases. In order to quantify this phenomenon, we report in Figure 5 the evolution of both Ba(α) and Ba(β) as a function of the temperature through the representation of the binding energy differences $|Ba(\alpha) - Ti\ 3p|$ and $|Ba(\beta) - Ti\ 3p|$, to reduce uncertainties and the evolution of $|Ba(\alpha) - Ba(\beta)|$ to allow a direct comparison with theoretical results. Figure 5(B) shows the results for the Ba(β) component, which is related to the first surface layer, as previously demonstrated;[25] while Figure 5(A)

displays the results for the Ba(α) component, related to phenomena taking place in deeper layers.

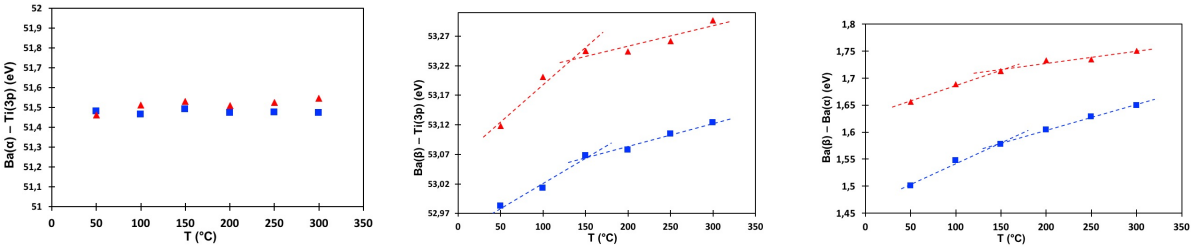

(A) (B) (C)

Figure 5: Experimental evolution of binding energy differences of (A) $|Ba(\alpha) - Ti\ 3p|$ (B) $|Ba(\beta) - Ti\ 3p|$ and (C) $|Ba(\alpha) - Ba(\beta)|$ as a function of temperature (in °C). Values for sample 1 (10 nm of $BaTiO_3$) are reported with blue squares, while red triangles stand for sample 2 (16 nm of $BaTiO_3$). Dotted lines are linear regression used as eye guidelines below or above 150°C.

Let us first discuss the behavior of the Ba $4d$ lines components. It is worth noting that both Ba(α) and Ba(β) components are present at all temperatures, including those well above the ferroelectric-paraelectric phase transition Curie temperature. This means that even in the paraelectric phase, $BaTiO_3$ still exhibits two Ba chemical environments. This observation allows to definitely exclude the possibility that these two Ba components arise from different ferroelectric domains as was previously suggested.[35] According to Figure 5(A), whatever the sample thickness is, no significant evolution can be observed for the $|Ba(\alpha) - Ti\ 3p|$ difference with respect to the temperature. On the contrary, the behavior differs significantly for $|Ba(\beta) - Ti\ 3p|$, and thus also for $|Ba(\alpha) - Ba(\beta)|$ differences (see Figure 5(B) and (C)). Since $|Ba(\alpha) - Ti\ 3p|$ is almost constant, let us focus on the discussion of the $|Ba(\alpha) - Ba(\beta)|$ difference. This latter increases with temperature for both samples. However, a marked slope change appears around 150°C. To highlight this effect, tendency curves with linear regression are plotted for both temperature domains (*i.e.* below/above 150°C) in Figure 5. This eyes guideline helps to identify the slope break. Measures of the slopes lead to values significantly different for lines related to evolution below ($\approx 7\ 10^{-4}$ eV/K) and above 150°C ($\approx 3.5\ 10^{-4}$ eV/K). For both samples, this break occurs around 150

°C, which is a temperature close to the Curie temperature of $BaTiO_3$ (130°C).

In order to compare experimental and theoretical results, let us analyze the relative slopes in the two identified temperature regions. According to the work of Han *et al.*,[36] the dilation coefficient of the ferroelectric phase is 6.83 10^{-5} Å/K, while for the paraelectric phase it is equal to 1.57 10^{-4} Å/K. Thanks to these dilatation coefficients, one can convert the experimental slopes derived from Figure 5(C) to enable the comparison with the theoretical results. We find slopes of 10.2 eV/Å and 2.2 eV/Å for the ferroelectric and the paraelectric phases, respectively. These values suffer from a series of approximations and limitations making direct comparison with theoretical values (6.9 and 0.6 eV/Å, respectively) difficult. First, the dilatation coefficients considered here are the ones of bulk $BaTiO_3$ which may not be equivalent for thin films, although it may provide clues to expected trends in relative evolution between the ferro and paraelectric phases. Moreover, our films are deposited on a substrate which has its own dilatation coefficient. This later is likely to modify the intrinsic dilatation coefficient of $BaTiO_3$ epitaxial films, probably not in the same way for 10 nm and 16 nm thick films given the nanoparticle size dependence reported by Han *et al.*[36] This could give an explanation for the binding energy shift observed between both samples. Indeed, thickness by itself could not be the origin of the shift, as calculations carried out on samples of different thicknesses (from 7 to 13 layers) show identical results. Finally, although the experimental and theoretical slope values do not match perfectly, their trends are similar and consistent, confirming a drastic reduction of the slope above the ferroelectric transition as a potential signature of the ferro-paraelectric transition.

Discussion

Before going further, a basic interpretation can be proposed to explain the observed behavior. The energy of an electron, either from Ba(α) or Ba(β) is directly related to the orbital energy (ϵ_α or ϵ_β) but also to the electric field induced by local polarization. Indeed, in an electric

field defined by an electrostatic potential V, a charge q has an energy equal to qV, which is directly related to the potential, itself related to the electric field. The electron energy can thus be written as follows:

$$E^{\alpha/\beta}_{electron} = \epsilon_{\alpha/\beta} - e \times V^{\alpha/\beta}_{POL}$$

with $V^{\alpha/\beta}_{POL}$ the electrostatic potential induced by ferroelectricity. Given our previous results[26] on $BaTiO_3$ or the ones of Gattinoni *et al.*[37] on $PbTiO_3$, surface polarization is reduced as compared to the bulk one, we can thus write $V^{\beta}_{POL}=\gamma \times V^{\alpha}_{POL}$ with $\gamma < 1$. Knowing that the binding energy of Ba(β) is larger than the one of Ba(α), the evolution of the binding energy of an electron emitted from Ba(β) or Ba(α) atoms can be schematically represented as depicted in Figure 6, with respect to temperature and/or ferroelectric polarization strength. It explains well why the difference between β and α levels decreases (respectively increases) when the ferroelectric polarization increases (respectively when the temperature increases).

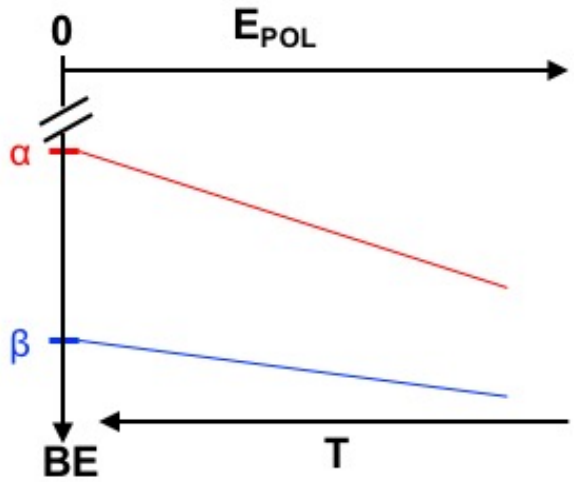

Figure 6: Schematic evolution of the energy of an electron extracted from a Ba(α) or from a Ba(β) atom as a function of the ferroelectric polarization strength (through E_{POL}) and of the temperature.

In order to rationalize this behavior, electronic structure analysis has been performed for the paraelectric and ferroelectric phases. Densities of states (DOS) have been calculated and

the results for Ba (surface and bulk) and Ti atoms are reported in Figure 7. No significant

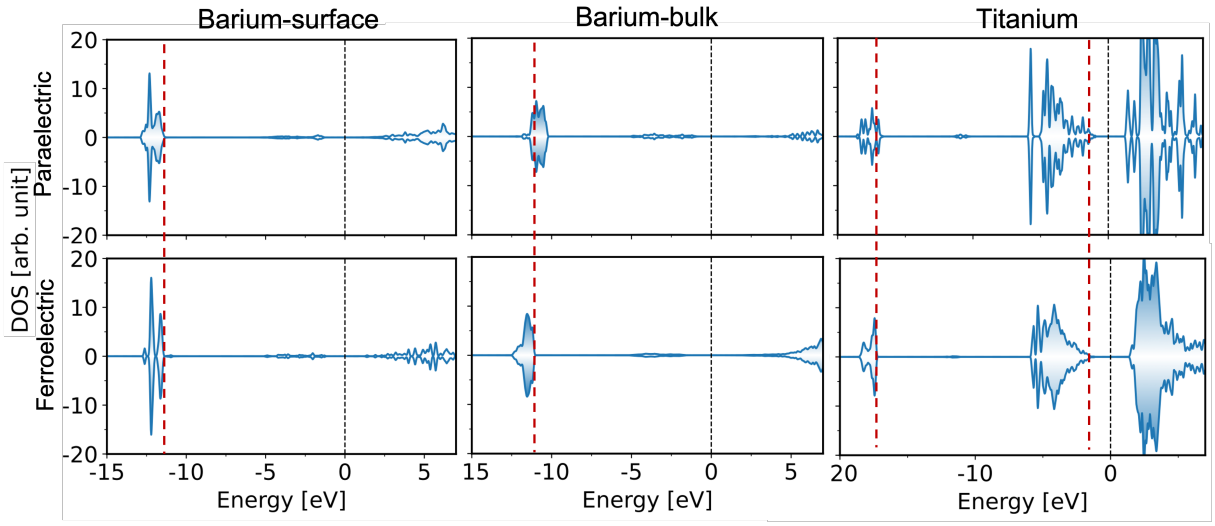

Figure 7: Densities of states (DOS) for (Top) paraelectric and (Bottom) ferroelectric slabs for surface and bulk Ba and Ti atoms. Dotted black lines stand for the Fermi level, while dotted red lines are guidelines to evidence evolution between the two phases.

change is observed for oxygen atoms. According to Figure 7, surface barium atoms are not affected by the phase transition. To the contrary, occupied states of both bulk Ba and Ti atoms are shifted towards higher energies during the transition from the ferroelectric to the paraelectric state. This electronic analysis demonstrates that the phase transition mostly impacts bulk atoms. The DOS shift towards higher energy levels indicates the decrease in effective nuclear charge experienced by the valence electrons, which results in a shift of the PES binding energy towards lower values. Now we understand that the apparent stability observed in Figure 5 for Ba(α) - Ti $3p$ conceals a synergetic evolution of Ti and bulk Ba atoms while the Ba(β) - Ti $3p$ evolution is only due to the Ti atoms, with surface Ba atoms remaining stable. More generally, our study confirms the loss, recently reported for $PbTiO_3$,[37] of ferroelectric polarization in the surface region, due to depolarization, as compared to the polarized core of the film. Thus, this may be a general behavior for ferroelectric films.

To go further, the different bulk versus surface behavior of titanate ferroelectrics can also be interpreted in terms of crystal-field splitting of Ti $3d$ orbitals. Indeed, in agreement

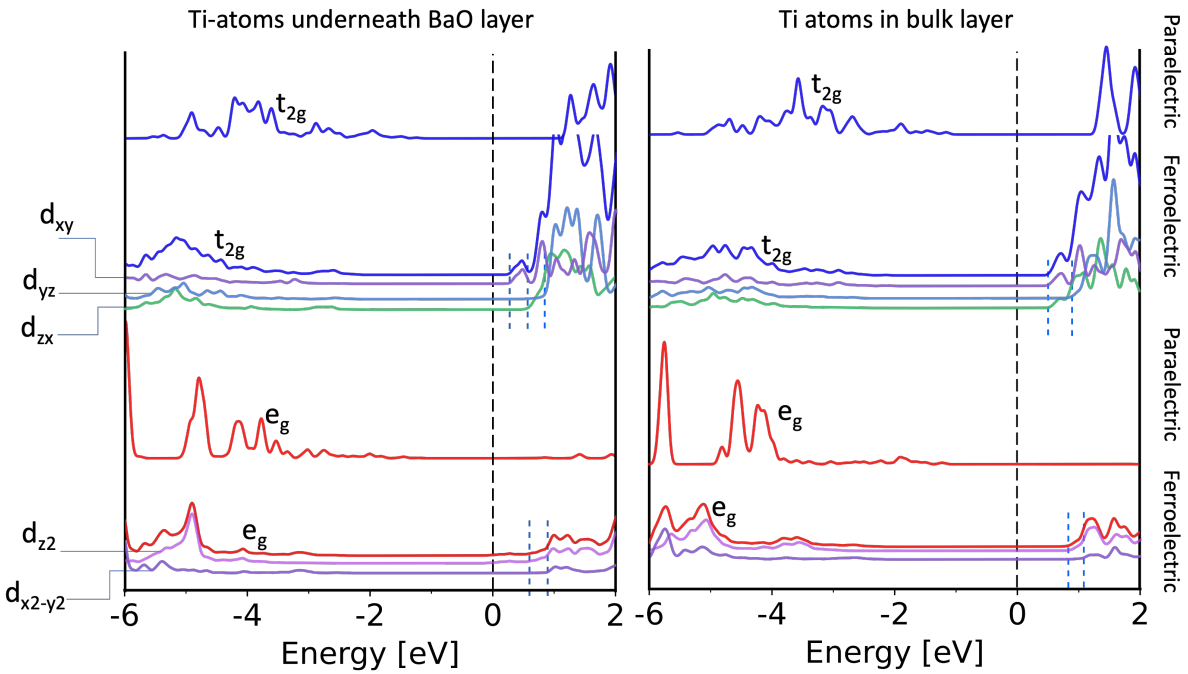

Figure 8: Projected densities of states (DOS) for Ti-atoms present in the bulk layer (Right) and in the layer underneath BaO (Left) for ferroelectric and paraelectric cases. Dotted black lines tand for the Fermi level, while blue dotted lines highlight the energy splitting difference among d-orbitals.

with previous results on $CaTiO_3$[38] and as it can be observed in Figure 8, the Ti $3d$ orbitals split into two levels (t_{2g}, e_g) in the cubic (*i.e.* paraelectric) structure. To the contrary, in the ferroelectric phase, this degeneracy is lifted due to a change in symmetry from cubic to tetragonal, where orbitals are further split into four sublevels (d_{xy}=d_{zx}, d_{yz}, d_{z^2}, $d_{x^2-y^2}$) for bulk TiO_2 layer and five (d_{xy}, d_{zx}, d_{yz}, d_{z^2}, $d_{x^2-y^2}$) for TiO_2 ones underneath the terminal BaO layer. These modifications in degeneracy in Ti$3d$ levels observed between ferro and paraelectric phases and between TiO_2 underneath surface and bulk TiO_2 layers might also be behind the observed splitting of Ba $4d$ core levels and their variation with temperature and strain. The validity of this hypothesis implies that one should be able to observe the influence of ferroelectricity on d orbitals of A atoms of other $ATiO_3$ compounds. Therefore, we chose to apply the same theoretical procedure as the one described for $BaTiO_3$ on two other compounds: $SrTiO_3$ (another well-known ferroelectric compound) and $RaTiO_3$ (an hypothetical compound, with A from the same column than Ba and Sr in the table of

elements). By analogy with $BaTiO_3$, we consider signals from $3d$ and $5d$ orbitals for $SrTiO_3$ and $RaTiO_3$, respectively, and we analyze the difference between PES signals from surface atoms (called β, like for $BaTiO_3$) and bulk atoms (called α). Corresponding results are reported in Figure 9.

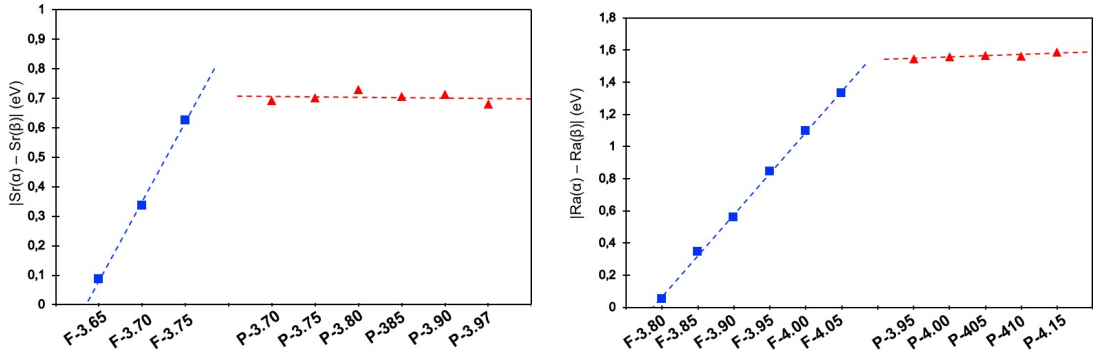

Figure 9: Theoretical evolution of (Left) $|Sr(\alpha)-Sr(\beta)|$ (in eV) and (Right) $|Ra(\alpha)-Ra(\beta)|$ as a function of ferroelectricity and lattice parameter. For values in abscissa, F stands for a ferroelectric slab, while P corresponds to the paraelectric one. Numbers next to P or F indicate the lattice parameter in Å. Blue squares stand for the values for ferroelectric slabs and red triangles stand for paraelectric slabs. Blue and red dotted lines are eye guidelines and correspond to linear regressions for ferro and paraelectric data, respectively.

According to these figures, it clearly appears that the change of slope of core level energy differences, as a function of strain between ferro and paraelectric phases is a general behavior of $ATiO_3$ compounds. Therefore, for these compounds, one can use the present experimental approach, *i.e.* use the $|A(\alpha)-A(\beta)|$ photoemission peaks energy difference dependence with temperature in order to determine the ferro-paraelectric phase transition.

Conclusion

In summary, DFT calculations on $BaTiO_3$ have demonstrated that the evolution of core-level binding energy shifts of the Ba $4d$ components is strongly dependent on the ferro/paraelectric state and for the ferroelectric phase, it strongly depends on the strain level. To confirm these results, we have investigated single crystalline $BaTiO_3$ thin films, with controlled surface terminations. Additionally, PES is a suitable technique to probe the surface of the films,

thanks to the splitting of the Ba $4d$ peak into two components representative of either the bulk (Ba(α)) or the extreme surface (Ba(β)) of the film. Working at low photon energy allowed us to investigate only the first atomic layers of the surface. We demonstrated that upon increasing temperature, the topmost layer is not affected in the same manner than deeper layers. By combining these observations with DOS calculations, we demonstrate that the extreme surface does not face any modification during phase transition, while inner "bulk" atoms (both Ba and Ti) are impacted. These experimental results confirm our DFT conclusions and thus demonstrate that PES can be used as a probe for the ferroelectric to paraelectric phase transition. This phenomena is not restricted to $BaTiO_3$ and can easily be extended to other $ATiO_3$ ferroelectric compounds at least. Besides according to our results on the ferroelectric phase, one could follow the strength of electrical polarization by recording the core level difference between Ba(β) and Ti $3p$. These observations are believed important for understanding the ferroelectric behavior of devices generally made of thin films.

Acknowledgement

This work was supported by the ANR PHOTO-POT project, grant ANR-15-CE05-0014 of the French Agence Nationale de la Recherche. The authors also thank the ANR for financial support through project ANR-17-EURE-0002 (EIPHI Graduate School). The research leading to this result has been supported by the project CALIPSOplus under the Grant Agreement 730872 from the EU Framework Program for Research and Innovation HORIZON 2020. Calculations were performed using HPC resources from DNUM CCUB (Centre de Calcul de l'Université de Bourgogne). This work was also granted access to the HPC resources of IDRIS under the allocation 2022-A0130811108 made by GENCI.

Supporting Information Available

Survey scans corresponding to sample cleaning as well as example of peaks decomposition are reported in Supplementary Information.

References

(1) Chang, Y.; Xue, R.; Wang, Y. Multilayered Barium Titanate Thin Films by Sol-Gel Method for Nonvolatile Memory Application. *IEEE Trans. Electron Devices* **2014**, *61*, 4090–4097.

(2) Bin, C.; Hou, X.; Wang, K.; Liao, L.; Xie, Y.; Yang, H.; Wei, H.; Liu, Y.; Wang, J. Interlayer Coupling Enhanced Energy Storage Performance in a Flexible BMT-BTO/BMT Multilayer Ferroelectric Film Capacitor. *ACS Appl. Mater. & Interfaces* **2022**, *14*, 50880–50889.

(3) Miao, Z.; Chen, L.; Wang, R.; Yuan, R.; Zhou, F.; Lv, P.; Zhang, X.; Wang, Q. Gold nanoparticles decorated on $BaTiO_3$ as photocatalyst: effect of SPR and ferroelectricity. *Mater. Res. Express* **2018**, *5*, 025505.

(4) Xue, K.; Jiang, Y.; Mofarah, S.; Doustkhah, E.; Zhou, S.; Zheng, X.; Huang, S.; Wang, D.; Sorrell, C.; Koshy, P. Composition-driven morphological evolution of $BaTiO_3$ nanowires for efficient piezocatalytic hydrogen production. *Chemosphere* **2023**, *338*, 139337.

(5) von Hippel, A.; Breckenridge, R.; Chesley, F.; Tisza, L. High dielectric constant ceramics. *Ind. Enf. Chem.* **1946**, *38*, 1097–1109.

(6) Kwei, G. H.; Lawson, A. C.; Billinge, S. J. L.; Cheong, S. W. Structures of the ferroelectric phases of barium titanate. *J. Phys. Chem.* **1993**, *97*, 2368–2377.

(7) Smith, M. B.; Page, K.; Siegrist, T.; Redmond, P. L.; Walter, E. C.; Seshadri, R.; Brus, L. E.; Steigerwald, M. L. Crystal Structure and the Paraelectric-to-Ferroelectric Phase Transition of Nanoscale $BaTiO_3$. *J. Am. Chem. Soc.* **2008**, *130*, 6955–6963.

(8) Rabuffetti, F. A.; Brutchey, R. L. Structural Evolution of $BaTiO_3$ Nanocrystals Synthesized at Room Temperature. *J. Am. Chem. Soc.* **2012**, *134*, 9475–9487.

(9) Yashima, M.; Hoshina, T.; Ishimura, D.; Kobayashi, S.; Nakamura, W.; Tsurumi, T.; Wada, S. Size effect on the crystal structure of barium titanate nanoparticles. *J. Appl. Phys.* **2005**, *98*, 014313.

(10) Page, K.; Proffen, T.; Niederberger, M.; Seshadri, R. Probing Local Dipoles and Ligand Structure in $BaTiO_3$ Nanoparticles. *Chem. Mater.* **2010**, *22*, 4386–4391.

(11) Polinger, V.; Garcia-Fernandez, P.; Bersuker, I. Pseudo Jahn–Teller origin of ferroelectric instability in $BaTiO_3$ type perovskites: The Green's function approach and beyond. *Phys. B: Condens. Matter* **2015**, *457*, 296–309.

(12) Panchal, G.; Choudhary, R. J.; Yadav, S.; Phase, D. M. Probing the effect of ferroelectric to paraelectric phase transition on the Ti-3d and O-2p hybridization in $BaTiO_3$. *J. Appl. Phys.* **2019**, *125*, 214102.

(13) Hickox-Young, D.; Puggioni, D.; Rondinelli, J. M. Persistent polar distortions from covalent interactions in doped $BaTiO_3$. *Physical Review B* **2020**, *102*, 014108.

(14) Shiratori, Y.; Pithan, C.; Dornseiffer, J.; Waser, R. Raman scattering studies on nanocrystalline $BaTiO_3$ Part I - Isolated particles and aggregates. *J. Raman Spectrosc.* **2007**, *38*, 1288–1299.

(15) Mishra, V.; Sagdeo, A.; Kumar, V.; Warshi, M. K.; Rai, H. M.; Saxena, S. K.; Roy, D. R.; Mishra, V.; Kumar, R.; Sagdeo, P. R. Electronic and optical properties

of $BaTiO_3$ across tetragonal to cubic phase transition: An experimental and theoretical investigation. *J. App. Phys.* **2017**, *122*, 065105.

(16) El Marssi, M.; Le Marrec, F.; Lukyanchuk, I. A.; Karkut, M. G. Ferroelectric transition in an epitaxial barium titanate thin film: Raman spectroscopy and x-ray diffraction study. *J. App. Phys.* **2003**, *94*, 3307–3312.

(17) Ravel, B.; Stern, E. A.; Vedrinskii, R. I.; Kraizman, V. Local structure and the phase transitions of $BaTiO_3$. *Ferroelectrics* **1998**, *206*, 407–430.

(18) Kresse, G.; Furthmüller, J. Efficiency of ab-initio total energy calculations for metals and semiconductors using a plane-wave basis set. *Comput. Mater. Sci.* **1996**, *6*, 15 – 50.

(19) Kresse, G.; Furthmüller, J. Efficient iterative schemes for ab initio total-energy calculations using a plane-wave basis set. *Phys. Rev. B* **1996**, *54*, 11169–11186.

(20) Kresse, G.; Joubert, D. From ultrasoft pseudopotentials to the projector augmented-wave method. *Phys. Rev. B* **1999**, *59*, 1758–1775.

(21) Perdew, J.; Burke, K.; Ernzerhof, M. Generalized Gradient Approximation Made Simple. *Phys. Rev. Lett.* **1996**, *77*, 3865–3868.

(22) Dudarev, S. L.; Botton, G. A.; Savrasov, S. Y.; Humphreys, C. J.; Sutton, A. P. Electron-energy-loss spectra and the structural stability of nickel oxide: An LSDA+U study. *Phys. Rev. B* **1998**, *57*, 1505–1509.

(23) Suzuki, K.; Kijima, K. Optical Band Gap of Barium Titanate Nanoparticles Prepared by RF-plasma Chemical Vapor Deposition. *Jpn. J. Appl. Phys.* **2005**, *44*, 2081–2083.

(24) Pack, J.; Monkhorst, H. "Special points for Brillouin-zone integrations"—a reply. *Phys. Rev. B* **1977**, *16*, 1748–1749.

(25) Deleuze, P.; Magnan, H.; Barbier, Z., A. Li; Verdini, A.; Floreano, L.; Domenichini, B.; Dupont, C. Nature of the Ba 4*d* Splitting in $BaTiO_3$ Unraveled by a Combined Experimental and Theoretical Study. *J. Phys. Chem. C* **2022**, *126*, 15899.

(26) Deleuze, P.-M.; Mahmoud, A.; Domenichini, B.; Dupont, C. Theoretical investigation of the platinum substrate influence on $BaTiO_3$ thin film polarisation. *Phys. Chem. Chem. Phys.* **2019**, *21*, 4367.

(27) Barbier, A.; Mocuta, C.; Stanescu, D.; Jegou, P.; Jedrecy, N.; Magnan, H. Surface composition of $BaTiO_3/SrTiO_3(001)$ films grown by atomic oxygen plasma assisted molecular beam epitaxy. *J. App. Phys.* **2012**, *112*, 114116.

(28) Kvasov, A.; Tagantsev, A. Role of high-order electromechanical coupling terms in thermodynamics of ferroelectric thin films. *Phys. Rev. B* **2013**, *87*, 184101–184111.

(29) Fairley, N.; Fernandez, V.; Richard-Plouet, M.; Guillot-Deudon, C.; Walton, J.; Smith, E.; Flahaut, D.; Greiner, M.; Biesinger, M.; Tougaard, S.; *et al.*, Systematic and collaborative approach to problem solving using X-ray photoelectron spectroscopy. *Appl. Surf. Sci. Adv.* **2021**, *5*, 100112/1–100112/9.

(30) Köhler, L.; Kresse, G. Density Functional Study of CO on Rh(111). *Phys. Rev. B* **2004**, *70*, 165405/1–165405/9.

(31) Zhong, W.; King-Smith, R.; Vanderbilt, D. Giant LO-TO Splittings in Perovskite Ferroelectrics. *Phys. Rev. Lett.* **1994**, *72*, 3618.

(32) Dronskowski, R.; Bloech, P. Crystal orbital Hamilton populations (COHP): energy-resolved visualization of chemical bonding in solids based on density-functional calculations. *J. Phys. Chem.* **1993**, *97*, 8617.

(33) Maintz, S.; Deringer, V.; Tchougreff, A.; Dronskowski, R. Analytic projection from

plane-wave and PAW wavefunctions and application to chemical-bonding analysis in solids. *J. Comput. Chem.* **2013**, *34*, 2557.

(34) Nelson, R.; Ertural, C.; George, J.; Deringer, V.; Hautier, G.; Dronskowski, R. LOBSTER: Local orbital projections, atomic charges, and chemical-bonding analysis from projector-augmented-wave-based density-functional theory. *J. Comput. Chem.* **2020**, *41*, 1931.

(35) Kumar, S.; Raju, V. S.; Kutty, T. R. N. Investigations on the chemical states of sintered barium titanate by X-ray photoelectron spectroscopy. *App. Surf. Sc.* **2003**, *206*, 250–261.

(36) Han, M.; Rong, Y.; Li, Q.; Xing, X.; Kang, L. Thermal expansion of nano-sized $BaTiO_3$. *Cryst. Eng. Comm.* **2015**, *17*, 1944.

(37) Gattinoni, C.; Strkalj, N.; Härdi, R.; Fiebig, M.; Trassin, M.; Spaldin, N. Interface and surface stabilization of the polarization in ferroelectric thin films. *Proc. Natl. Acad. Sci. U.S.A.* **2020**, *117*, 28589–28595.

(38) Cao, Y.; Park, S. Y.; Liu, X.; Choudhury, D.; Middey, S.; Meyers, D.; Kareev, M.; Shafer, P.; Arenholz, E.; Chakhalian, J. Orbital configuration in $CaTiO_3$ films on $NdGaO_3$. *Applied Physics Letters* **2016**, *109*, 152905.

TOC Graphic

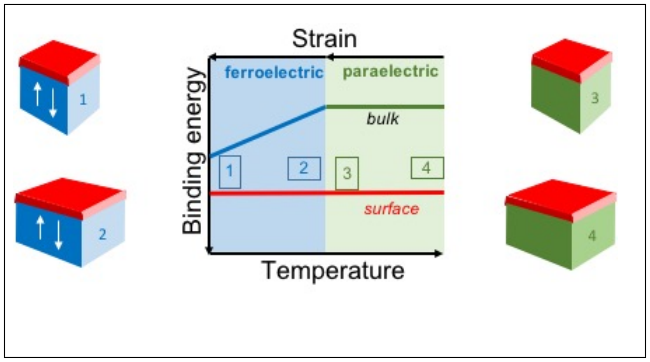
Strain
ferroelectric
paraelectric
bulk
surface
Binding energy
Temperature
1
2
3
4